Ductile-Brittle Transition Temperatures and Dynamic Fracture Toughness of 9Cr-1Mo Steel

A. MOITRA, P.R. SREENIVASAN, S.L. MANNAN, and V. SINGH

The ductile-brittle transition temperature (DBTT) of 9Cr-1Mo steel was characterized by an RT_{NDT}-based K_{IR} curve approach and a reference temperature (T_0)-based master curve (MC) approach. The MC was developed at a dynamic loading condition (loading rate of 5.12 m/s), using precracked Charpy V-notch (PCVN) specimens, and the reference temperature was termed T_0^{dy}. The RT_{NDT} and T_0^{dy} were determined to be −25 °C and −52 °C, respectively. The T_0^{dy} was also estimated from instrumented CVN tests, using a modified Schindler procedure to evaluate K_{Jd}; the result shows close agreement with that obtained from the PCVN tests. The ASME K_{IR}-curve approach proves to be too conservative compared to the obtained trend of the fracture toughness with temperature. The cleavage fracture stress, σ_f^*, estimated from the critical length, l^*, shows good agreement with that estimated from the load-temperature diagram (2400 to 2450 MPa), which was constructed from the CVN test results. The crack initiation mechanism has been identified as decohesion of the particle-matrix interface, rather than as the fracture of the particles.

I. INTRODUCTION

A number of fast breeder reactor (FBR) programs have placed major emphasis on the choice of ferritic-martensitic steels as wrapper material, due to the inherent high void swelling resistance of the steel at high damage doses.[1–6] For this application, the 9Cr-1Mo steel in tempered martensitic condition is one of the leading candidate materials.[7–10] However, being a ferritic steel, it is prone to temperature-dependent ductile-brittle transition in fracture mode, and the irradiation-induced rise of the transition temperature is a matter of concern, especially under dynamic/accidental loading during a fuel-handling operation. According to a recent study, with respect to handling requirements, the transition temperature of the irradiated wrapper material should be below 200 °C.[11] Because of this, it is essential to examine the ductile-brittle transition temperature (DBTT) of the unirradiated steel based on its dynamic fracture toughness (DFT), especially in the transition temperature regime.

In describing the DBTT, the RT_{NDT}-based K_{IR} curve[12,13] approach is purely empirical and based on the data obtained from reactor pressure vessel steels only. However, it is now well understood that the size, shape, and distribution of the carbides ahead of the crack tip leads to scatter in fracture toughness; the empirical description of its temperature dependence may lead to nonrealistic assessment of the fracture resistance of the material in the transition temperature regime. A description of the fracture mechanism through a "weakest link" theory,[14] and the subsequent modeling of scatter using a three-parameter Weibull distribution, has led to the development of the master curve (MC),[15–21] which describes the temperature dependence of fracture toughness for the ferritic steels, indexed by a material-specific reference temperature, T_0. The MC provides significant technical enhancement over the empirically determined K_{IR} curve, as T_0 is evaluated from the direct determination of the fracture toughness. The ASTM E 1921-97[22] has standardized the process of evaluating both the T_0 and the MC for ferritic steels, under quasi-static loading conditions. However, its application to higher strain rates needs further verification and validation through DFT evaluation. In this article, the reference temperature, T_0, and the MC have been determined for a 9Cr-1Mo steel in the dynamic loading condition, using precracked Charpy V-notch (PCVN) specimens. The term T_0^{dy} has been used instead of T_0 to signify dynamic loading; the MC thus determined is referred to as the "master curve from dynamic fracture toughness (MC-DFT)." The potential for using conventional CVN tests to estimate the reference temperature has also been explored. The MC-DFT thus determined has been compared with the RT_{NDT}-based ASME K_{IR} curve. The results would permit the evaluation of the DBTT of 9Cr-1Mo steel in terms of DFT. The cleavage fracture mechanisms involved in this temperature regime have also been discussed.

II. MATERIAL

The 20-mm-thick plate of 9Cr-1Mo steel was supplied by M/s Creusot-Loire Industrie (France). The detailed chemical composition (wt pct) is given as C: 0.10, Cr: 8.44, Mo: 0.94, Ni: 0.17, Cu: 0.10, Si: 0.48, S: 0.002, P: 0.007, Al: 0.011, and Fe: the balance. The plate was normalized at 950 °C for 30 minutes and then tempered at 750 °C for 60 minutes. This treatment gives rise to a tempered lath martensitic structure for 9Cr-1Mo steel.[32]

III. EXPERIMENTAL

The RT_{NDT} of the material has been determined by the drop weight and Charpy tests, as suggested in the ASME specifications.[12,13] The drop-weight tests were carried out according to ASTM E-208[23] specifications, with P-2 (20-mm-thick)

A. MOITRA and P.R. SREENIVASAN, Scientific Officers, and S.L. MANNAN, Director, are with the Metallurgy and Materials Group, Indira Gandhi Centre for Atomic Research, Kalpakkam, Tamilnadu 603 102, India. V. SINGH, Professor, is with the Department of Metallurgical Engineering, Banaras Hindu University, Varanasi, India. Contact e-mail: moitra@igear.ernet.in

Manuscript submitted June 22, 2004.

specimens. Both long (2-in.) and short (1-in.) crack-starter weld beads were used. The Charpy tests were carried out with standard-sized (10 × 10 × 55 mm) CVN specimens, following the ASTM E 23 guideline.[24]

The T_0^{dy} of the material has been determined following the ASTM E 1921 guideline.[22] The DFT (K_{Jd}) was determined from the precracked Charpy test. To avoid inertial oscillations, tests were conducted at a lower hammer velocity (~1.12 m/s). For the different specimens, the variation of the test velocity was restricted within ±1 pct. The ASTM E 1921 suggests that the test temperature should be selected such that it yields fracture toughness values (corresponding to 1-in. thickness specimens) close to 100 MPa $\sqrt{m}$. According to this guideline, following some trial and error tests, 50 °C was selected as the test temperature. The initial crack length was measured by a traveling microscope, using the 10-point averaging method {(9 points from interior + mean from 2 surface crack lengths)/10}. As discussed afterwards, the T_0^{dy}, determined at a hammer velocity of ~1.12 m/s has further been converted to T_0^{dy} corresponding to 5.12 m/s applying a test velocity dependent shift in T_0. The T_0^{dy} was also estimated from instrumented CVN tests, using a modified Schindler procedure to evaluate K_{Jd}, as discussed in Section IV–B–2.

To identify the micromechanism involved in the fracture process, scanning electron microscopy (SEM) was carried out on the fracture surfaces from the precracked specimens.

IV. COMPARISON OF THE ASME K_{IR} CURVE AND THE MC-DFT

A. *Determination of the* RT_{NDT} *and* K_{IR} *Curve*

1. *Determination of* RT_{NDT}

The reference temperature currently used for reactor pressure vessel steels is RT_{NDT}.[12,13] The RT_{NDT} is defined as the higher of the two temperatures T_{NDT} and (T_{CV} −33 °C), where T_{NDT} is the drop-weight nil-ductility temperature and T_{CV} is the temperature at which both the CVN energy of 68 J and a lateral expansion of 35 mils (1 mils = 0.001 in.) are obtained. To prevent catastrophic brittle fracture in the components, it is recommended that the operating temperature be 33 °C or more above the RT_{NDT}, depending on the component thickness.

The T_{NDT} for the 9Cr-1Mo steel was determined from drop-weight tests to be −25 °C. The break/no-break results obtained at different test temperatures are shown in Table I. Figure 1 shows the variation of the Charpy impact energy with temperature for the 9Cr-1Mo steel. Figure 2 shows the variation in the lateral expansion with temperature. According to the ASME specification,[12,13] the points representing the lowest Charpy energy or lateral expansion at each temperature were fitted by a fit-curve (a sigmoidal fit, in the present case), as shown in Figures 1 and 2. The transition temperatures corresponding to the Charpy 68 J energy and the 35 mils lateral expansion were determined to be −32 °C and −31 °C, respectively. Thus, following the ASME criterion, the higher of these two temperatures, *i.e.*, −31 °C, was determined to be the T_{CV}. Thus, the RT_{NDT} of 9Cr-1Mo steel has been determined to be the higher of the two temperatures T_{NDT} and (T_{CV} −33 °C), *i.e.*, −25 °C.

2. *Determination of the* K_{IR} *Curve*

The ASME code (Section III, Div. I, Appendix G) gives the reference toughness curve, known as the "K_{IR} curve,"

Table I. The Break/No-Break Results from Drop-Weight Tests

	Specimen	Test Temperature (°C)	Break/ No Break	Conclusion
Long weld bead	1L	−20	no break	T_{NDT} = −25 °C
	2L	−20	no break	
	3L	−25	no break	
	4L	−30	break	
	5L	−50	break	
	6L	−25	break	
	7L	−25	break	
	8L	−40	break	
Short weld bead	1S	−20	no break	T_{NDT} = −25 °C
	7S	−20	no break	
	9S	−30	break	
	10S	−25	no break	
	11S	−25	break	
	12S	−30	break	

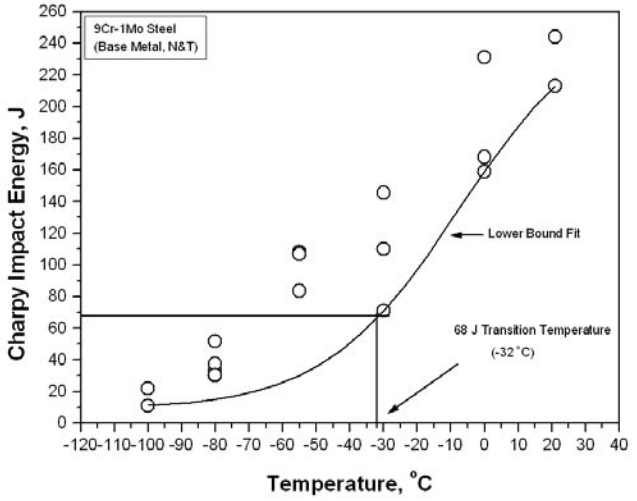

Fig. 1—Charpy impact energy *vs* test temperature of the 9Cr-1Mo base material.

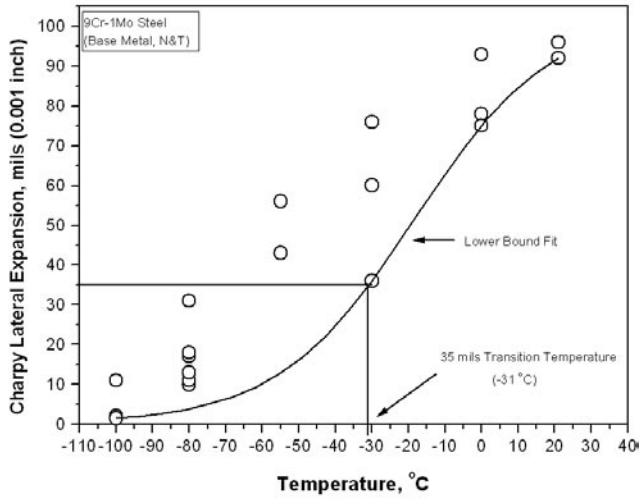

Fig. 2—Variation of the lateral expansion variation, with test temperature for 9Cr-1Mo base material.

indexed with the RT_{NDT} of the material, in the form of the following equation:

$$K_{IR} = 29.4 + 13.675 * \exp(0.026 * (T - RT_{NDT})) \quad [1]$$

where K_{IR} is in MPa$\sqrt{m}$ and T is the temperature in degrees Celsius. As discussed earlier, the K_{IR} curve empirically describes the lower limit of the fracture toughness transition with respect to temperature for pressure vessel steels. This encompasses static fracture toughness, K_{IC}; DFT, K_{Id}; and crack arrest toughness, K_{IA}, in the transition temperature regime for the material. The K_{IR} curve thus determined has been compared with the MC-DFT in Figure 6.

B. *Determination of the* T_0 *and the Dynamic MC*

1. T_0^{dy} *from Pre Cracked Charepy Test (PCVN)*

Figure 3 shows a typical load-displacement plot for 9Cr-1Mo steel, obtained from a PCVN test at −50 °C. This shows clear elastic-plastic fracture with substantial work hardening before the fracture load is reached. Using these traces, the DFT, K_{Jd}, was determined from the PCVN tests, following the ASTM E 1921[22] guideline. The validity of each K_{Jd} datum was examined by the validity limit equation, as given in

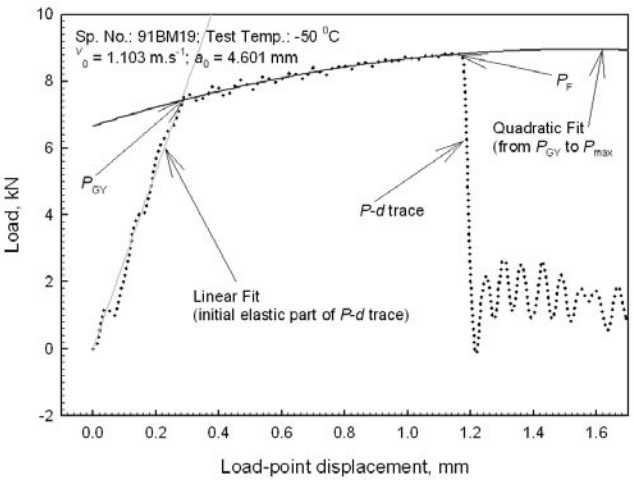

Fig. 3—Typical load-displacement plot from PCVN tests at −50 °C for 9Cr-1Mo base material.

$$K_{Jd} \le \left[\frac{Eb_0\sigma_{yd}}{30}\right]^{0.5} \quad [2]$$

where E is the Young's modulus, b_0 is the remaining ligament length, and σ_{yd} is the dynamic yield stress. The equations given in ASTM E 1921[22] were used to determine the validity limits, the scale parameter of the Weibull distribution, and T_0^{dy}, except the static fracture toughness term, K_{Jc}, was replaced by its dynamic counterpart, K_{Jd}. However, for the sake of clarity, relevant equations are stated in the discussion.

The test temperature, test velocity, validity limits, and 1-in.-corrected K_{Jd} values are reported in Table II. The 1-in. equivalence of each K_{Jd} value was estimated using

$$K_{Jd(2)} = K_{min} + [K_{Jd(1)} - K_{min}]\left(\frac{B_1}{B_2}\right)^{\frac{1}{4}} \quad [3]$$

where K_{min} is 20 MPa$\sqrt{m}$, the subscript 2 refers to specimens 1-in. (25.4-mm) thick, and the subscript 1 refers to the tested specimen thickness (10 mm, in the present case).

Two tests were conducted at a hammer velocity of 5.12 m/s at −20 °C, and the corresponding results are also shown in Table II. As suggested in ASTM E-1921, the invalid values, truncated at the validity limit, were used for further processing, along with the valid K_{Jd} values.

The scale parameter of the Weibull distribution, K_0, was estimated following[22]

$$K_0 = \left[\sum_{i=1}^{N}(K_{Jd(i)} - K_{min})^4/(N - 0.3068)\right]^{1/4} + K_{min} \quad [4]$$

where the K_{min} is 20 MPa$\sqrt{m}$ and N is the number of tests included in the calculation.

Table II. The K_{Jd} Results from PCVN Tests for the 9Cr-1Mo Base Material at Hammer Velocity of ~1.12 m/s

Specimen	Test Temp. (°C)	Initial Test Velocity V_0 (m·s^{-1})	Initial Crack Length, a_0 (mm)	K_{Jd} (MPa·$\sqrt{m}$)	σ_{yd} (MPa)	Validity Limit, (MPa·$\sqrt{m}$)	Validity Results	1-in.-Size Corrected K_{Jd} (MPa·$\sqrt{m}$)
91BM11	−70	1.08	4.408	57.8	—	—	—	49.0
91BM13	−55	1.066	4.427	56.4	—	—	—	48.8
91BM12	−50	1.111	4.505	137.1	717.3	166.1	valid	112.8
91BM14	−50	1.113	4.395	162.3	707.6	166.6	valid	132.7
91BM15	−50	1.147	4.707	186.0	742.6	165.9	invalid	152.2*
91BM16	−50	1.151	4.383	83.5	713.6	167.5	valid	70.3
91BM17	−50	1.1267	4.61	118.9	745.6	167.7	valid	98.3
91BM18	−50	1.143	4.541	P_F not clear	717	165.5	—	—
91BM19	−50	1.103	4.601	243.9	721.6	165.2	invalid	197.3*
91BM10	−50	1.103	4.805	60.0	$P_F < P_{GY}$	—	valid	51.7
91BM20	−50	1.131	4.885	163.0	762.5	165.2	valid	136.4
91BM8	−50	1.107	5.095	70.0	$P_F < P_{GY}$	—	valid	60.0
91BM9	−50	1.127	4.632	133.9	712.1	163.6	valid	110.3
91BM21	−20	5.12	4.870	286.7	779.7	166.7	invalid	230.6*
91BM22	−20	5.12	4.625	296.5	789.2	171.6	invalid	233.4*

*The 1-in. size is corrected from invalid K_{Jd}.

Taking into account all the valid and invalid K_{Jd} values (not 1-in.-size-corrected) obtained at −50 °C, K_0 has been determined 149.65 MPa$\sqrt{\text{m}}$. After a 1-in. size correction, K_0 was found to be 122.70 MPa$\sqrt{\text{m}}$.

Using 122.70 MPa$\sqrt{\text{m}}$ as the K_0, the median K_{Jd} (where the probability of failure is 0.5) and the reference temperature for the MC, T_0^{dy}, were calculated using, respectively,

$$K_{Jd(\text{med})} = (K_0 - K_{\min})[\ln (2)]^{\frac{1}{4}} + K_{\min} \quad [5]$$

$$T_0 = T - \frac{1}{0.019} \ln\left[\frac{K_{Jd(\text{med})} - 30}{70}\right] \quad [6]$$

Thus, the $K_{Jd(\text{med})}$ was determined to be 113.71 MPa$\sqrt{\text{m}}$. Using −50 °C as the test temperature (T) and $K_{Jd(\text{med})}$, the T_0^{dy} was determined to be −59.4 °C.

The cumulative probability of failure, p_f, corresponding to the DFT values was assessed following Eq. [7] [ASTM E 1921], after ranking the values by increasing order of magnitude.

$$p_f = (i - 0.3)/(N + 0.4) \quad [7]$$

where i is the rank of the corresponding K_{Jd} value (i = 1 for the lowest K_{Jd} and i = N for the highest K_{Jd}) and N is the total number of K_{Jd} values (10, in the present case). The Weibull plot, as constructed with all the valid and invalid K_{Jd} values (the invalid values were truncated at the corresponding validity limits) obtained from the tests at −50 °C, is shown in Figure 4. Following ASTM E-1921, a regression line with a fixed slope 4 was fitted to the data points (shown in Figure 4) following the form

$$Y = 4X + Y_0 \quad [8]$$

where

$$Y_0 = -4 \ln (K_0 - 20) = -19.45$$

Out of 10 data points, 7 were found to lie on the forced fit (with a slope 4) line. Following ASTM E 1921 (Section X3.1), for the fixed slope of 4 and with $K_{\min}$ as 20 MPa$\sqrt{\text{m}}$, the standard deviation was calculated to be 26.23 MPa$\sqrt{\text{m}}$.

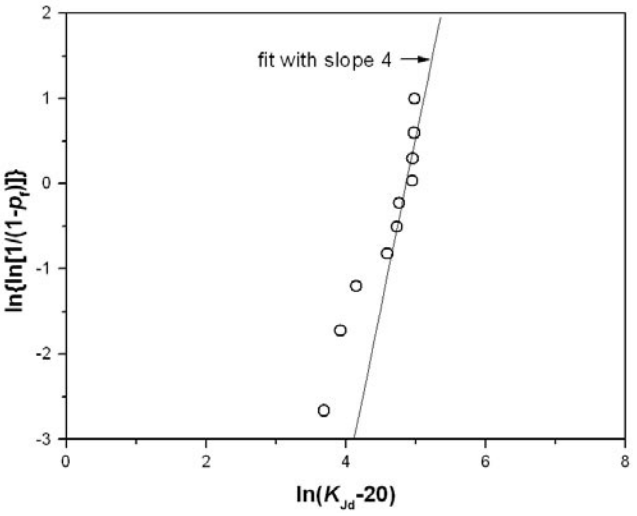

Fig. 4—Weibull plot with all the K_{Jd} data, obtained from PCVN test at −50 °C, with a hammer velocity of ~1.12 m/s.

For the reasons mentioned earlier, the PCVN tests were conducted at a reduced velocity of ~1.12 m/s. To account for the test velocity effect on the reference temperature, T_0, among various equations proposed by Yoon *et al.*,[25] the following represent the highest and the lowest values, respectively.

For A515 steel,

$$T_0 = 6.1 \ln (dK/dt) - 18 \quad [9a]$$

and for A533B weld,

$$T_0 = 2.7 \ln (dK/dt) - 87 \quad [9b]$$

where dK/dt is the stress intensity factor rate expressed in MPa$\sqrt{\text{m}}$/s, and T is expressed in degrees Celsius.

In a more generalized form, Schindler *et al.*[26] have proposed the following equation for the shift in T_0, associated with the change in test velocity or the stress intensity factor rate as

$$\Delta T \cong (22 - 0.016\sigma_y) \log \frac{\dot{K}_{\text{ref}}}{\dot{K}_{\text{test}}} \cong (22 - 0.016\sigma_y) \log \frac{\dot{V}_{\text{ref}}}{\dot{V}_{\text{test}}} \quad [10]$$

where σ_y is the yield stress at the test temperature/strain rate expressed in MPa; $\dot{K}_{\text{ref}}/\dot{K}_{\text{test}}$ is $(dK/dt)_{\text{ref}}/(dK/dt)_{\text{test}}$, where dK/dt is expressed in MPa$\sqrt{\text{m}}$/s; and $\dot{V}_{\text{ref}}/\dot{V}_{\text{test}}$ is $\text{velocity}_{\text{ref}}/\text{velocity}_{\text{test}}$.

For the PCVN tests conducted at −50 °C, the stress intensity factor rate (dK/dt) was estimated to be 2.754(±0.254) · 10^5 MPa$\sqrt{\text{m}}$/s at the loading rate ~1.12 m/s. For the loading rate 5.12 m/s, the estimated stress intensity factor rate was ~10^6 MPa$\sqrt{\text{m}}$/s. Applying these dK/dt values in Eq. [9a], the T_0 was found to be 14 °C more for tests at 5.12 m/s than at 1.12 m/s. Similarly, from Eq. [9b], the shift was found to be 6.2 °C. However, Eq. [10] shows a shift of ~7 °C from the dK/dt-based calculation and 7.5 °C from the velocity-based estimation. It is important to mention here that the dynamic yield stress estimation from the PCVN tests gives a higher value than that estimated from the CVN tests at a particular temperature.[27] Here, using Eq. [10], the yield stress estimated from CVN tests, 660 MPa at −50 °C, was used to arrive at a conservative estimate (a higher ΔT) of shift.

From the various estimates mentioned for the test-velocity-induced shifts in T_0, it is observed that the Schindler's[26] velocity-based estimation (Eq. [10]) is more tangible from a practical point of view; considering the scatter involved in all the test parameters used in determining T_0, the result seems to be reasonable. So, the T_0^{dy} corresponding to the test velocity of 5.12 m/s has been determined to be T_0^{dy} (at ~1.12 m/s) + 7.5 °C ~ −52 °C. The MC at the test velocity of 5.12 m/s (MC-DFT) has been plotted using −52 °C as the T_0^{dy}.

2. *The* T_0^{dy} *from the CVN tests*

The T_0^{dy} from the CVN tests was estimated from the K_{Jd} values at different temperatures. The K_{Jd} values have been estimated from the J_{Id}, where the J_{Id} values were evaluated from the load-displacement plots and the absorbed Charpy energy using Eq. [11], proposed by Schindler:[28,29]

$$J_0 = \frac{7.33 \cdot n \cdot C_V \cdot 10^{-3}}{1 - 1.47 \cdot \left(\frac{C_V}{\sigma_{fd}}\right)} \quad [11]$$

The original equation was proposed by Schindler[28] and later modified by Sreenivasan *et al.*,[29] where the work-hardening exponent n was determined directly from the load-displacement diagram obtained from the instrumented CVN tests alone. Figure 5 shows the typical load-displacement plot, obtained from the Charpy test at −80 °C. The K_{Jd} results obtained from Charpy tests at different temperatures are shown in Table III. It is to be noted that the Schindler method[28,29] is applicable to ductile metals with CVN energy >30 to 40 J and with good work hardening.

After estimating the K_{Jd} from the C_V values by the method discussed earlier, the resulting K_{Id} data have been processed according to the ASTM E 1921 procedure. For determining the validity limit, considering the notch depth was 2 mm for standard CVN specimens, the remaining ligament length, b_0, was taken to be 8 mm. Then the K_{Jd} values obtained were converted to adjust for a 1-in.-sized specimen. The validity limits and the 1-in.-size-corrected K_{Jd} is reported in Table IV.

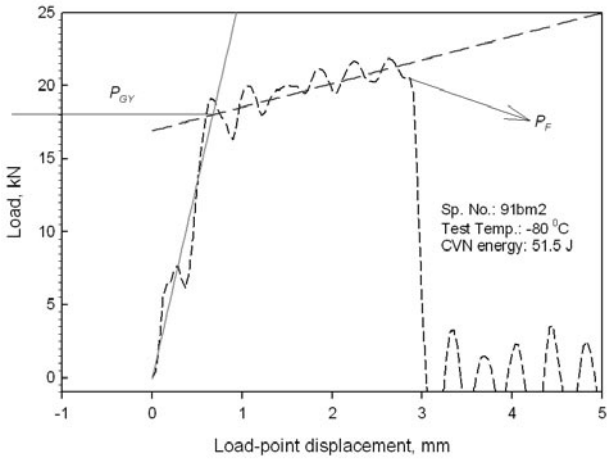

Fig. 5—Typical load-displacement trace for 9Cr-1Mo base material from CVN test at −80 °C.

An exponential fit was drawn through the 1-in.-size-corrected and valid K_{Jd} data, and the T-K_{Jd} pairs from 80 to 120 MP$\sqrt{\text{m}}$ were selected and analyzed for evaluating the reference temperature, using Eq. [12], as proposed by Wallin:[19]

$$0 = \sum_{i=1}^{i=n} \frac{\delta_i \exp\{0.019(T_i - T_0)\}}{[31 - K_{\min} + 77 \exp\{0.019(T_i - T_0)\}]} - \sum_{i=1}^{n} \frac{(K_{Jdi} - K_{\min})^4 \exp\{0.019(T_i - T_0)\}}{[31 - K_{\min} + 77 \exp\{0.019(T_i - T_0)\}]^5} \quad [12]$$

where the Kronecker $\delta_i = 1$ for valid data and 0 for noncleavage or censored data. The term $K_{\min} = 20$ MPa$\sqrt{\text{m}}$.

This procedure yields a T_0^{dy} of −30 °C with only the valid K_{Jd} values. However, as observed in Figure 7, even the invalid K_{Jd} values (except one) lie within the tolerance bounds of the MC-DFT. Thus, a fit was also drawn through all the valid and invalid K_{Jd} values, and a value of −47.3 °C was obtained, which has been in close agreement with the T_0^{dy} determined earlier from the PCVN tests (−52 °C). From these results, it is concluded that the use of conventional CVN specimens has good potential for developing MC; however, this procedure needs to be further refined with tests using a variety of materials.

3. *Construction of the Dynamic MC*

Following Ortner's[30] proposition, it is expected that under dynamic loading conditions, the MC would follow the same shape as in the quasi-static case, because the increase in yield stress would be compensated for by the decrease in the strain-hardening exponent. Hence, in the

Table III. Estimated DFT (K_{Jd}) of 9Cr-1Mo Base Metal from CVN Specimens

Test Temp. (°C)	CVN Energy (J)	Yield Load, P_{GY} (kN)	$(P_{max} + P_{GY})/2$ P_{max} = Maximum Load	Dynamic Work-Hardening Exponent, n	Yield Stress, from P_{GY}, σ_{yd} (MPa)	Flow Stress, $(P_{max} + P_{GY})/2$ or σ_{fd} (MPa)	K_{Jd} (MPa$\sqrt{\text{m}}$)
−100	22.0	19.50	—	—	911.0	—	77.3*(P_F)
−100	11.0	—	—	—	—	—	—
−100	11.0	—	—	—	—	—	—
−80	51	18.0	20.0	0.0644	840.9	933.0	74.8
−80	30	19.0	20.1	0.0488	887.7	941.0	49.3
−80	30	18.0	19.2	0.0362	840.9	897.0	42.1
−80	33	17.5	19.4	0.0374	817.6	907.7	45.0
−80	37	17.8	19.6	0.0453	831.6	913.4	53.0
−80	30	18.0	19.9	0.0313	840.9	927.4	39.5
−55	83.5	17.0	19.2	0.0657	794.2	896.0	99.0
−55	108	—	—	—	—	—	—
−55	107	14.1	17.7	0.1100	658.7	825.5	149.7
−30	145	15.3	17.7	0.0817	714.8	826.5	156.8
−30	110	15.0	17.9	0.0650	704.0	838.1	116.5
−30	71	15.5	17.9	0.0800	724.1	838.6	315.2
0	231	14.0	16.5	0.1102	654.0	771.3	262.8
0	159	15.0	17.5	0.0650	700.8	817.6	148.3
0	168	—	—	—	—	—	—
21	213	13.5	16.5	0.1145	630.7	771.8	248.9
21	244	14.3	16.9	0.0946	668.0	790.5	252.6

*Schindler's J_d estimation process is applicable for $C_V > 30$ to 40.

Table IV. The 1-in.-Size-Corrected K_{Jd} Results for the Valid Values

Test Temperature (°C)	K_{Jd} (MPa$\sqrt{m}$)	ASTM E-1921 Validity Limit, (MPa·$\sqrt{m}$)	Validity Results	1-in.-Size Corrected K_{Jd} (MPa·$\sqrt{m}$)
−100	77.3*(P_F)	227.4	valid	65.4
−80	74.8	217.9	valid	63.4
−80	49.3	223.9	valid	43.2
−80	42.1	217.9	valid	37.5
−80	45.0	214.9	valid	39.8
−80	53.0	216.7	valid	46.1
−80	39.5	217.9	valid	35.4
−55	99.0	211.0	valid	82.6
−55	149.7	192.2	valid	122.8
−30	156.8	199.6	valid	128.3
−33	116.5	198.0	valid	96.4
−30	315.2	200.9	invalid	253.8*
0	262.8	190.1	invalid	212.3*
0	148.3	196.8	valid	121.6
21	248.9	186.1	invalid	201.3*
21	252.6	191.6	invalid	204.2*

*Invalid 1-in.-size-converted data.

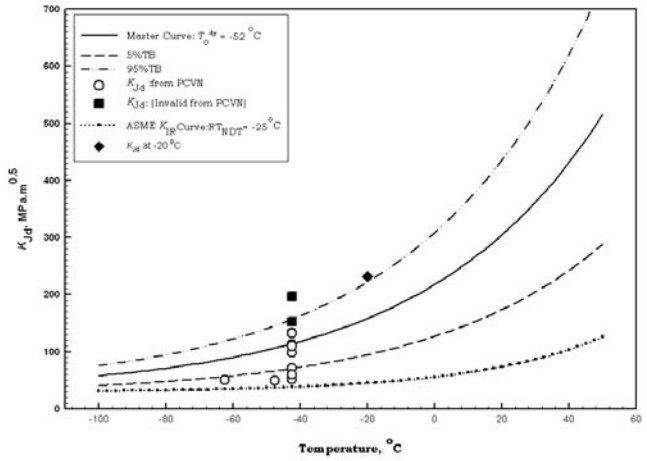

Fig. 6—Dynamic MC (at 5.12 m/s) and ASME K_{IR} curve for 9Cr-1Mo base material.

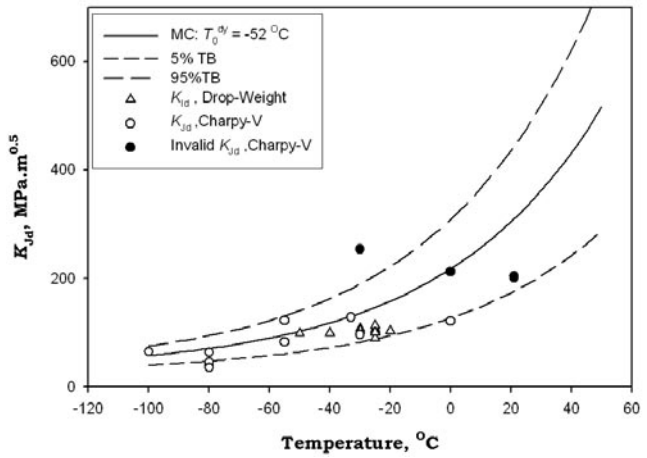

Fig. 7—Dynamic MC (at 5.12 m/s) and K_{Jd} and K_{Id} values obtained from CVN specimens.

present study of developing the MC for 9Cr-1Mo steel under a dynamic loading condition, the MC equations corresponding to static/quasi-static cases were used, as suggested in ASTM E 1921, except the static toughness terms were replaced by their dynamic counterpart, *i.e.*, K_{Jd}. Equation [13] provides the MC-DFT and Eqs. [14] and 15 provide the 5 and 95 pct tolerance bounds (TBs) for the MC-DFT.

$$K_{Jd}\,(\text{median}) = 30 + 70 \exp\,(0.019(T - T_0^{dy})) \quad [13]$$

$$K_{Jd}\,(5\text{ pct TB}) = 25.4 + 37.8 \exp\,(0.019(T - T_0^{dy})) \quad [14]$$

$$K_{Jd}\,(95\text{ pct TB}) = 34.6 + 102.2 \exp\,(0.019(T - T_0^{dy})) \quad [15]$$

Using the reference temperature obtained from PCVN tests (T_0^{dy}), −52 °C, the MC-DFT corresponding to 5.12 m/s and its 5 and 95 pct TB have been constructed and shown in Figures 6 and 7. In Figure 6, the MC-DFT is compared with the ASME K_{IR} curve drawn according to Eq. [1], using −25 °C as the RT_{NDT}. Following the shift of 7.5 °C applied to T_0^{dy} (to account for the rate differences between the actual PCVN test velocity of 1.12 m/s and the usual CVN test velocity of 5.12 m/s), the temperatures corresponding to the PCVN K_{Jd} results were also shifted by 7.5 °C in the temperature scale. The K_{Jd} values obtained from the CVN tests (as discussed in Section IV–B–2) are superimposed on the MC-DFT and shown in Figure 7. Figure 7 also shows the K_{Id} values for the same steel, determined earlier by the authors, using instrumented drop-weight tests.[31,32] Compared to the MC-DFT along with its TBs, the ASME K_{IR} curve proves to be too conservative. The DFT trends determined by all the methods discussed earlier (PCVN, CVN, and drop-weight tests) reasonably agree with the MC-DFT trend, but they all lie much above the trend of the K_{IR} curve through the entire DBTT regime. In Figure 7, as discussed earlier, the trend in the K_{Jd} values obtained from the CVN tests shows good agreement with the MC-DFT; even the invalid values (except one) lie within the TB of the MC. Thus, the reference temperature determined from CVN tests to be −47.3 °C (from the fit incorporating all the valid and invalid data) seems reasonable. The K_{Id} values obtained from the drop-weight tests[31,32] are proven to be conservative with respect to MC-DFT.

V. THE CLEAVAGE FRACTURE MECHANISM IN 9Cr-1Mo STEEL

In pursuit of a model to explain the relationship between the microscopic cleavage fracture and the macroscopic fracture toughness, Ritche *et al.*[33] have suggested that the applied tensile stress has to exceed the critical cleavage fracture stress, σ_f^*, over a critical microstructural distance, l^*. Here, σ_f^* corresponds to the cleavage fracture stress over the appropriate microstructural scale and l^* represents the probable separation between the crack tip and appropriately configured microcrack nucleation sites. In continuation, Odette *et al.*[34] proposed the following relationship with the fracture toughness and l^*, based on the finite-element-based assessment of stress distribution ahead of a blunt crack by McMeeking:[35]

$$\sigma_f^* = \sigma_0[A_i - (B_i l^* \sigma_0)/(K_{IC})^2] \quad [16]$$

where K_{IC} is the static fracture toughness and σ_0 is the static yield stress. The term A_i is a unit less constant and B_i is a constant with a unit of stress (MPa) that depends on the strain-hardening exponent, n.

In the present study, the σ_f^* for the 9Cr-1Mo steel was estimated using Eq. [16], where the static values were replaced by their dynamic counterparts, K_{Jd} and σ_{yd}, respectively, where K_{Jd} is the DFT and σ_{yd} is the dynamic yield stress. Odette *et al.*[34] give A_i and B_i values for various ranges of n values. For the present analysis, A_i and B_i were taken to be 4 and 100, respectively, assuming the n is 0.1 in all cases. The l^* was directly measured from the fracture surfaces of the broken specimens under a scanning electron microscope; it is the minimum distance from the fatigue-cracked front to the cleavage-initiating point. The cleavage-initiating point was identified by back-tracking the cleave lines directly under the scanning electron microscope. A typical example of the l^* measurement is shown in detail in Figures 8(a) and (b). Only those precracked specimens yielding valid K_{Jd} data (as given in Table II) were considered for the σ_f^* estimation. The cleavage fracture stress thus estimated is given in Table V.

In another attempt, the cleavage fracture stress for the 9Cr-1Mo steel was estimated from the load-temperature diagram constructed by the yield load, P_{GY}, the fracture load, P_F, and the maximum load, P_{max}, variation with temperature, as derived from the instrumented CVN tests. The load-temperature diagram for the 9Cr-1Mo steel is shown in Figure 9. The general methods for analyzing such diagrams have been discussed in detail in the literature.[36,37] At the brittle transition temperature T_D, where $P_F = P_{GY}$, cleavage fracture strength or microcleavage fracture stress is given by

$$\sigma_f^* = C_F \sigma_{Yd} \quad [17]$$

where C_F is the stress intensification factor. For a full-sized Charpy V-notch (FCVN) specimen, C_F values ranging from 2.40 to 2.57 have been reported at T_D. The selection of either the Tresca or the Von Mises yield criterion can introduce a difference of 10 pct.

From the load-temperature diagram, the brittleness transition temperature (where $P_F = P_{GY}$) was identified as −105 °C and the corresponding load as 20.4 kN. Thus, from Eq. [17], the cleavage fracture stress was estimated to be 2400 to 2450 MPa. The estimations of cleavage fracture stress, σ_f^*, from PCVN test results using Eq. [16] and from the load-temperature diagram using CVN test results, show good agreement. This, in turn, supports the concept of the existence of a critical stress criterion over a critical distance in controlling the fracture in this low-temperature regime.

To gain more insight into the micromechanism of fracture of this steel, the fracture morphology at the critical distance was further examined with SEM. A typical SEM fractograph, observed at the critical distance in a precracked sample, is shown in Figure 10. The fractographic features show that the

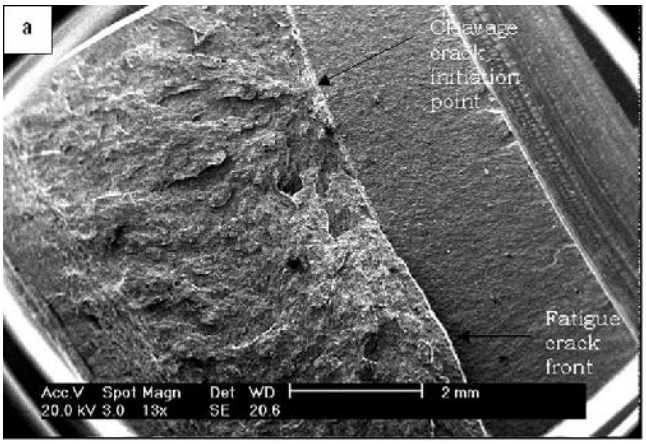

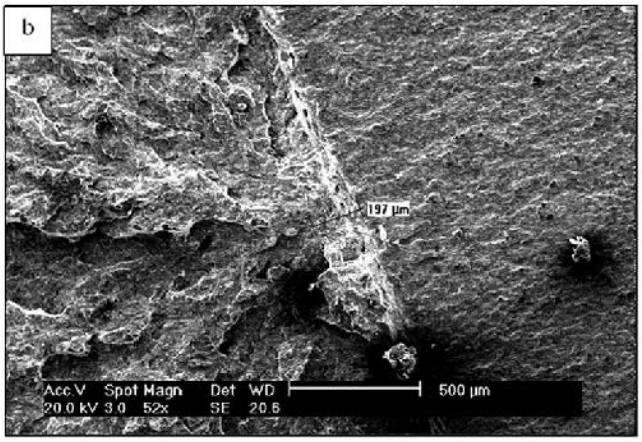

Fig. 8—Estimation of critical microstructural distance for cleavage crack initiation, l^*, from SEM, at (*a*) lower magnification and (*b*) higher magnification (specimen 91BM14).

Table V. The σ_f^* Results from PCVN Tests for the 9Cr-1Mo Steel

Specimen	K_{Jd} (MPa·$\sqrt{m}$)	l^* (μm)	σ_f^* (MPa)
91BM12	137.1	88.5	2695.6
91BM14	162.3	197	2400.8
91BM16	83.5	77.7	2449.7
91BM17	118.9	119	2633.2
91BM10	60	41.4	2518.3
91BM20	163	194	2826.1
91BM8	70	139.5	2163.2
91BM9	133.9	127	2592.8

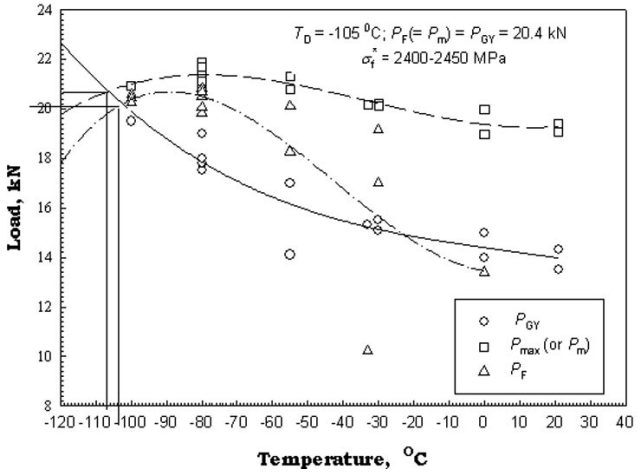

Fig. 9—Estimation of cleavage fracture stress from the load-temperature diagram, obtained from CVN tests (at 5.12 m/s).

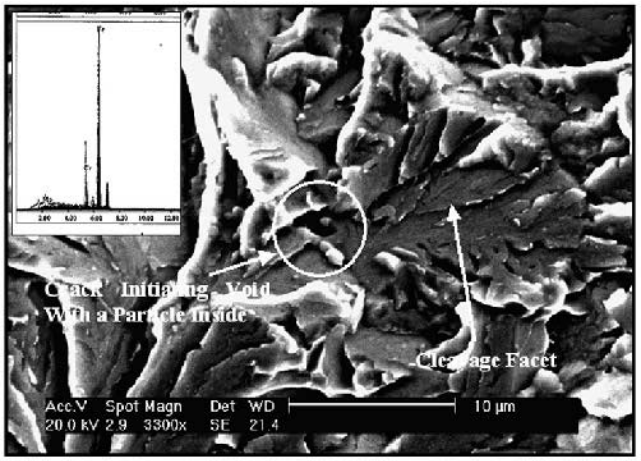

Fig. 10—Fractographs from the cleavage crack initiation site; at the marked region is a typical crack-initiating void with a particle inside (specimen 91BM12). Inset shows the EDX for the carbide.

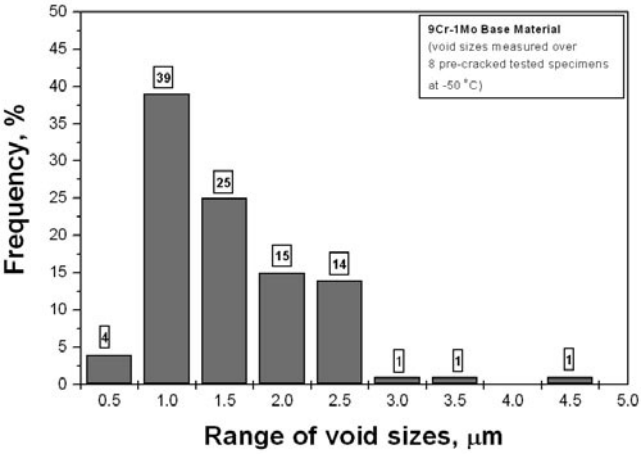

Fig. 11—Microvoid length distribution at the proximity of l^*.

crack had initiated at a void (marked by the circle) and further propagated by cleavage-exposing clear-cleavage facets (marked by the arrow). The microvoid, as marked in the picture, has originated around a particle and it appears that the void had initiated due to the particle-matrix decohesion rather than the fracture of the particle itself. Particles were found to be intact within the voids. The energy-dispersive X-ray (EDX) obtained from the particle (inset of Figure 10) shows that the particle was a Cr-rich carbide. The type of precipitate, generally found for this steel is of the Cr-rich $M_{23}C_6$ type.[32] Thus, the crack-initiating particle has been identified as $M_{23}C_6$ carbide.

The microvoid sizes, distributed in the proximity of l^*, were measured, and the microvoid length distribution over the eight precracked samples, tested at −50 °C, is shown in Figure 11. It is observed that the crack size occurring with maximum frequency (39 pct) is of ~1 μm, whereas the lowest crack size, ~4.5 μm, has a frequency of 1 pct. An effort was made to find out the void sizes responsible for the cleavage initiation; $(\sigma_f^*)^2/E$ was plotted against Q^{-1}, where σ_f^* is the cleavage fracture stress, E is the Young's modulus, and Q is the void size length. It was observed that, when the void sizes were taken from the maximum frequency band, the plot

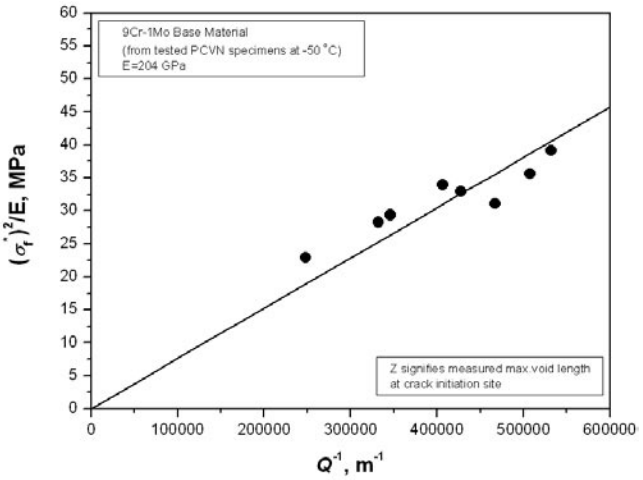

Fig. 12—Relationship between the maximum microvoid length (Q) and the cleavage fracture stress.

did not show a systematic relationship with the cleavage fracture stress; however, a linear trend was obtained when the maximum void sizes (with a frequency of 1 pct) were taken to obtain a fit. Figure 12 shows the $(\sigma_f^*)^2/E$ *vs* Q^{-1} plot, where Q is taken to be the maximum void sizes obtained from each specimen. The trend in Figure 12 indicates that the cleavage fracture stress is dependent on the maximum void size present at the critical distance from the fatigue-crack front. This closely resembles the Curry and Knott[38,39] model, which has postulated that none of the cracks, originating at the carbides contribute to the cleavage fracture initiation process, except for the top 5 pct size range (95th percentile). From Figure 12, therefore, it is concluded that only the voids with the maximum length have given rise to a cleavage fracture; this is in corroboration with the weakest link theory of fracture.[14]

VI. CONCLUSIONS

1. The T_0^{dy} determined for the 9Cr-1Mo steel at a loading rate of 5.12 m/s is −52 °C, whereas the RT_{NDT} is determined to be −25 °C. The ASME K_{IR} curve approach proves to be too conservative compared to the real trend of the fracture toughness with temperature, as shown by the dynamic MC.
2. The K_{Id} determined from the conventional CVN tests and the drop-weight tests follow the trend shown by the dynamic MC. The methodology suggested here for evaluating T_0^{dy} using only a CVN test bears potential, but needs to be verified with other materials.
3. The cleavage fracture stress, σ_f^*, estimated from the critical length, l^*, shows very good agreement with that estimated from the load-temperature diagram (2400 to 2450 MPa), constructed from CVN test results. This demonstrates the operation of a critical stress criterion over the critical distance in controlling the fracture toughness of this steel at the lower shelf.
4. The crack initiation mechanism is identified as the decohesion of the particle-matrix interface rather than as the fracture of the particle itself. The cleavage fracture stress is seen to be governed by the maximum void length

at the crack initiation site, rather than by the average size. This is in conformity with the weakest link theory.

REFERENCES

1. C. Brown, V. Levy, J.L. Seran, K. Ehrlich, R.J.C. Roger, and H. Bergmann: *Fast Reactors and Related Fuel Cycles-FR 91*, Atomic Energy Society, Tokyo, 1991, vol. 1.
2. C. Brown, R.J. Lilley, and G.C. Crittenden: *Nucl. Eng*., 1994, vol. 35, p. 122.
3. E. Materna-Morris and K. Ehrlich: *Proc. Technical Committee Meeting on Influence of High Dose Irradiation on Advanced Reactor Core Structural and Fuel Materials*, Obninsk, Russian Federation, 16–19 June 1997, IAEA-TECDOC-1039, August 1998, p. 129-138. ISSN. 1011-4289.
4. A.J. Lovell, A.I. Fox, W.H. Sutherland, and S.L. Hecht: *Reliable Fuels for Liquid Metal Reactors*, American Nuclear Society, LaGrange Park, IL, 1987, pp. 3-25.
5. V.S. Khabarov, A.M. Dvoriashin, and S.I. Porollo: *Proc. Technical Committee Meeting on Influence of High Dose Irradiation on Advanced Reactor Core Structural and Fuel Materials*, IAEA-TECDOC-1039, Vienna, 1998, p. 139.
6. S. Nomura, S. Shikakura, S. Ukai, I. Seshimo, M. Harada, I. Shibabara, and M. Katsuragawa: *Rast Reactors and Related Fuel Cycles-FR 91*, Atomic Energy Society, Japan, Tokyo, 1991, vol. 1.
7. J.L. Seran, V. Levy, P. Dubuisson, D. Gilbon, A. Maillard, A. Fissolo, H. Touron, R. Cauvin, A. Chalony, and E. Le Boulbin: *Proc. Int. Symp. on Effects of Radiation Materials*, ASTM STP 1125, N.H. Packan, R.S. Stoller, A.S. Kumar, and D.S. Gelles, eds., ASTM, West Conshohocken, PA, 1992, p. 1209.
8. A. Kohyama, A. Hishinuma, D.S. Gelles, R.L. Klueh, W. Dietz, and K. Ehrlich: *J. Nucl. Mater*., 1996, vols. 231–237, p. 138.
9. J.L. Seran, A. Alamo, A. Maillard, H. Touron, J.C. Brachet, P. Dubuisson, and O. Rabouille: *J. Nucl. Mater*., 1994, vols. 212–215, p. 588.
10. N.L. Hu. and D.S. Gelles: *Influence of Radiation on Material Properties*, ASTM, STP 956, 1987, p. 83.
11. *Preliminary Safety Analysis Report of PFBR*, Reactor Engineering Group, Indira Gandhi Centre for Atomic Research, Kalpakkan, India, 2002.
12. ASME Boiler and Pressure Vessel Code, Section III, *Nuclear Power Plant Components*, Div. 1, Appendix G, ASME, New York, NY, 1980.
13. ASME Boiler and Pressure Vessel Code, Section XI, *Rules for Inservice Inspection of Nuclear Power Plant Components*, Div. 1, Appendix A, ASME, New York, NY, 1980.
14. J.D. Landes and D.H. Shaffer: Scientific Paper No. 79-ID3-JINTF-P4, Westinghouse, Pittsburgh, PA, 1979.
15. K. Wallin, T. Saario, and K. Torroren: *Met. Sci*., 1984, vol. 18,p. 13.
16. K. Wallin: *Eng. Fract. Mech*., 1984, vol. 19. p. 1085.
17. K. Wallin: *Eng. Fract. Mech*., 1985, vol. 22, p. 149.
18. K. Wallin: *Proc. Joint IAEA/CSNI Specialist Meeting on Fracture Mechanics Verification by Large-Scale Testing*, NUREG/CP-0131 (ORNL/TM-12413), Oct. 1993, 1992 ORNL, Oak Ridge, TN, p. 465.
19. K. Wallin: *Advances in Fracture Research (Proc. Int. Conf. Fracture, ICF-9)*, B.L. Karihaloo, Y.W. Mai, M.I. Ripley, and R.O. Ritchie, eds., Sydney, Australia, 1997, vol. 5, p. 2333.
20. W. Server, S. Rosinski, R. Lott, C. Kim, and D. Weakland: *Int. J. Press. Ves. Piping*, 2002, vol. 79, p. 701.
21. B.Z. Margolin, V.A. Shvetsova, A.G. Gulenko, A.V Ilyin, V.A. Nikolaev, and V.I. Smirnov: *Int. J. Press. Ves. Piping*, 2002, vol. 79, p. 219.
22. *Test Method for Determination of Reference Temperature*, T_o, *for Ferritic Steels in the Transition Range*, ASTM E 1921–97, ASTM, West Conshohocken, PA, 1997.
23. *1990 Annual Book of ASTM Standards*, ASTM Standard E 208–87a, ASTM, West Conshohocken, PA, 1990, vol. 03.01, p. 360.
24. *1990 Annual Book of ASTM Standards*, ASTM Standard E 23–88, ASTM, West Conshohocken, PA, 1990, vol. 03.01, p. 197.
25. K.K. Yoon, J.B. Hall, Van Der Sluys, M. Higuchi, and K. Lida: *2001 ASME Pressure Vessel and Piping Conf*., Atlanta, GA, July 23–26, 2001, p. 1.
26. H.J. Schindler, T. Varga, D.H. Njo, and G. Prantl: *Materials Aging and Component Life Extension*, *Proc. Int. Symp. on Material Ageing and Component Life Extension*, Milan, Italy, Oct. 10–13, 1995, V. Bicego, A. Nitta, and R. Viswanathan, eds., vol. 2, p. 1367.
27. P.R. Sreenivasan and S.L. Mannan: *Int. J. Fract*., 2000, vol. 101, p. 229.
28. H.J. Schindler: *Pendulum Impact Testing: A Century of Progress*, ASTM STP 1380, ASTM, West Conshohocken, PA, 2000, p. 337.
29. P.R. Sreenivasan, C.G. Shastry, M.D. Mathew, K.B.S. Rao, S.L. Mannan, and G. Bandyopadhyay: *J. Eng. Mater. Technol. (Trans. ASME)*, 2003, vol. 125, p. 227.
30. S. Ortner: *Int. J. Press. Ves. Piping*, 2002, vol. 79, p. 693
31. A. Moitra, P.R. Sreenivasan, S.K. Ray, and S.L. Mannan: *Int. J. Press. Ves. Piping*, 1996, vol. 69, p. 253.
32. A. Moitra: Ph.D. Thesis, Banaras Hindu University, Varanasi, India, 2003.
33. R.O. Ritchie, J.F. Knott, and J.R. Rice: *J. Mech. Phys. Solids*., 1973, vol. 21, p. 395.
34. G.R. Odette and G.E. Lucas: *J. Nucl. Mat*., 1983, vol. 117, p. 264.
35. R.M. McMeeking: *J. Mech. Phys. Solids*, 1977, vol. 25, p. 357.
36. S.K. Ray, P.R. Sreenivasan, K.G. Samuel, and P. Rodriguez: *Int. J. Press. Ves. Piping*, 1993, vol. 54, p. 481.
37. R.A. Wullaert: *Impact Testing of Metals*, ASTM STP 466, ASTM, West Conshohocken, PA, 1970, p. 148.
38. D.A. Curry and J.F. Knott: *Met. Sci*., 1976, vol. 10, p. 1.
39. D.A. Curry and J.F. Knott: *Met. Sci*., 1978, vol. 12, p. 511.